JOURNAL OF GUIDANCE, CONTROL, AND DYNAMICS
Vol. 35, No. 4, July–August 2012

Regenerative Power-Optimal Reaction Wheel Attitude Control

Robin Blenden* and Hanspeter Schaub†
University of Colorado, Boulder, Colorado 80309

DOI: 10.2514/1.55493

This paper develops an analytical instantaneous power-optimal attitude control for a spacecraft using an integrated reaction wheel–flywheel system allowing for energy storage and return. The control is formulated in a general manner to use an arbitrarily large number of reaction wheels. It is applicable to systems with redundant wheels spanning three-dimensional space, which are controlled by a general attitude control law. The instantaneous power usage is minimized by modifying the wheel control torques using the wheel torque null motion. In this study, reducing the wheel speed results in negative power usage with perfect energy recuperation. Applying the maximum available wheel torque constraints, the null torque solution space is reduced to a hyperdimensional vector geometry problem, and the power-optimal wheel control torques are uniquely determined. The control modifications are applied to both attitude regulation and tracking control laws, demonstrating its performance for a variety of initial spacecraft states. Not only does the new control maximize the energy extraction from the reaction wheels, it also maintains the smallest flywheel spin rates, which helps reduce the maneuver-wide power usage.

I. Introduction

POWER is always a scarce resource on a spacecraft, and momentum exchange devices can be a considerable load [1]. While enhancing the performance of a particular subsystem generally requires design tradeoffs, optimal attitude control design can be applied to create power savings with few negative consequences. Power-optimal controls are of particular relevance for small spacecraft, which have been of great interest in recent years [2]. However, the electrical power usage is very limited on these small spacecraft as their small surface area limits how much heat can be radiated out to space. Furthermore, the use of power-optimal attitude controls systems, as well as integrated energy storage systems, can greatly increase the capability of such spacecraft in the near future [2,3].

A given control goal can often be achieved using a number of different implementations, allowing for substantial variation when optimizing control performance. When considering small spacecraft with limited resources, an important performance objective is the optimization of the attitude control system load on the power system. These power-optimal controls generally focus on minimizing the energy used over the course of an entire maneuver [4–6], although some aim to instantaneously minimize the power consumption [7]. There has been considerable interest (dating to the 1960s) in incorporation of energy storage capability into commonly used attitude control systems, since the reaction wheels and control-moment gyroscopes are ideal for use as flywheels. Flywheels are favorable when compared with chemical batteries for many other reasons, including extended lifetime and depth of discharge [3]. Application of integrated power and control systems (IPACS) could provide considerable spacecraft mass savings by eliminating some of the required capacity for chemical energy storage. Mechanical energy storage could provide a backup power system with no additional mass penalty, which would be of particular use during orbital eclipse and other periods of high demand on the energy storage systems. Because of dynamic constraints, flywheel systems are not generally well-suited to replace chemical batteries altogether, but they are useful for supplementing primary systems for power tracking and additional energy storage capacity [8,9].

A variety of control approaches have demonstrated the ability to simultaneously perform attitude control and useful power tracking [8]. By using the redundancy of the reaction wheels in conjunction with external thrusters, an arbitrary power profile may be tracked without interfering with the attitude control performance [3,10,11]. Reference [3] accomplishes this by decomposing the reaction wheel torques into two decoupled attitude control and power control components. By comparing power output against a desired power profile, this creates a more robust power tracking feedback control law [8]. However, this prior work has not examined the maximum amounts of energy that can be extracted if only a reaction wheel cluster is employed for attitude control. Energy extraction techniques have also been applied to variable-speed control-moment gyroscopes (VSCMGs), which provide an additional degree of control by allowing the flywheels to both gimbal and change their spin rate. By adapting techniques developed for singularity avoidance using the VSCMG reaction wheel mode [12], a similar result can be achieved [5].

In contrast, this paper presents a new method to minimize the instantaneous power usage where the spacecraft is controlled only using a cluster of reaction wheels. Of interest is how the reaction wheel motor torque null space is employed to achieve the smallest power usage at each control update time step. In [7], an analytical reaction wheel control solution is presented that minimizes the L_2 norm of the reaction wheel power requirements. In this scenario, no power extraction is obtained by spinning down any particular wheel. This paper expands this work to consider the ideal scenario of perfect power extraction when despinning a flywheel. As a result, the analytical solutions to the maximum bounds of how much power can extracted from or added to a reaction wheel cluster without impacting the attitude control stability requirements. Note that, in comparison with the results discussed in [3], the presented solution cannot track an arbitrary power profile because no external control torques are employed. However, having determined the range of power values that can be added or extracted from the momentum wheel cluster also allows for solutions that track a particular power profile within these bounds.

Both power-optimal controls and IPACS are of particular interest when designing small spacecraft. Small spacecraft are inexpensive and versatile, and recent interest in their applications has spurred development of more advanced attitude control systems to improve their capabilities [13]. In such spacecraft (generally with a mass less than 500 kg, and sometimes as little as 1 kg), mass and power budgets are particularly strict. With such limited available power, momentum exchange systems for attitude control are difficult to implement, making instantaneous power-optimal controls very important [7].

Received 1 July 2011; revision received 9 November 2011; accepted for publication 14 November 2011.

*Graduate Student, Aerospace Engineering Sciences Department.
†Associate Professor, H. Joseph Smead Fellow, Aerospace Engineering Sciences Department. Associate Fellow AIAA.

The incorporation of IPACS promises substantial mass savings (on the order of 50% for the combined power and attitude control systems), since chemical batteries generally consume a large portion of a small spacecraft's mass [14]. The work in this paper is very relevant to small spacecraft, since it applies an IPACS-type system to produce instantaneous power-optimal behavior not possible with a conventional reaction wheel system.

Power-optimal attitude control research applicable to reaction wheel systems focuses on minimizing the average power consumption over the course of a maneuver. Because the wheel motor power usage is the product of the wheel speed and wheel motor torque, the power consumption can be altered by changing either variable. Some strategies achieve the minimum power usage goal by working directly to minimize the integral of the wheel motor power over the course of a maneuver. By applying variational methods, the optimal wheel torque trajectory is determined numerically given a priori information about the initial and final states required by the maneuver [4]. In contrast, the present work is not considering maneuver-wide power-optimal solutions, as these require a priori knowledge of initial and final attitude states. Rather, the instantaneous power usage is sought to be minimized at each control step, analogous to the work in [7], employing a feedback control strategy.

Other strategies work to minimize energy usage indirectly without knowledge of the exact maneuver to be performed [15,16]. While only three reaction wheels are needed to produce a general three-axis control torque, many spacecraft carry at least one additional wheel for redundancy. Based upon design considerations, some, such as the Swift spacecraft, carry as many as six.[‡] Because of this redundancy, there are an infinite number of wheel torque solutions that apply the same net control torque onto the spacecraft. This fact can be used to formulate a new set of power-optimal controls for such redundant configurations.

A popular approach to reduce the energy usage of reaction wheel clusters is to constantly minimize all wheel speeds as a long-term strategy. These controls generally work by integrating the wheel speed error with respect to a minimum value (since a zero rate may be undesirable) and adjusting the wheel torque solution to constantly drive this error to zero [15,16]. This is useful to reduce net energy consumption but does not guarantee any instantaneous power performance. More recent research in [7] manipulates the motor torque null space to directly minimize the power consumption at any given instant. This instantaneous L_2 power-optimal control strategy is distinct from the maneuver-wide power reduction strategies methods above, because it guarantees optimal power use at any instant of time but does not consider long-term maneuver-wide power behavior. For practical applications, instantaneous and long-term power-optimal controls could be used in conjunction to produce the desired behavior, using the best qualities of each. This instantaneous L_2 power-optimal control provides the mathematical groundwork for the control presented here. In contrast with the solution in [7], the present work considers the scenario that despinning the flywheels allows for energy retrieval.

While spacecraft flywheel systems are a promising field of research, there are many technical challenges to be confronted. In addition to dynamics issues (such as power or attitude tracking singularities) affecting the control strategies described above, there are many hardware-related obstacles. The high speeds required (upward of 50,000 rpm) are demanding of the materials selected for the wheel, and they require use of composites to be feasible. The wheel bearings must also be exceptionally high-performance, generally requiring magnetic bearings. IPACS and other flywheel energy storage systems are actively being developed by NASA and the U.S. Air Force, among others, to tackle these challenges [3,8,10].

The paper outline is as follows. The rigid-body equations of motion considering a body-fixed cluster of reaction wheels is reviewed first. A sample attitude control strategy is presented, but the motor torque null space research is applicable for general attitude control strategies. After deriving the system dynamics and the regenerative reaction wheel control, a series of numerical maneuver simulations are presented. These demonstrate important aspects of the control's behavior for a variety of applications, comparing them with other relevant reaction wheel controls.

[‡]Data available at http://www.gdc4s.com/documents/Swift_RevE.pdf [retreived 2012].

II. Problem Statement

A. Definition of System

In this generalized rigid-body dynamics problem, the spacecraft body-fixed frame $\mathcal{B}$ is rotating with respect to the inertial frame $\mathcal{N}$, as illustrated in Fig. 1. Its total angular momentum may be decomposed into the separate momenta of the static components of the spacecraft $\mathbf{H}_b$ and its n arbitrarily oriented reaction wheels $\mathbf{H}_s$:

$$\mathbf{H} = \mathbf{H}_b + \mathbf{H}_s \tag{1}$$

Assuming that the spacecraft may be modeled as a rigid body with inertia tensor $[I]$, a constant when given in the $\mathcal{B}$ frame, the body angular momentum $\mathbf{H}_b$ is expressed in terms of $[I]$ and the body angular velocity $\boldsymbol{\omega}$ (the $\mathcal{B}$ frame angular velocity with respect to the inertial $\mathcal{N}$ frame) as

$$\mathbf{H}_b = [I]\boldsymbol{\omega} \tag{2}$$

The inertia tensor $[I]$ is assumed to account for all inertia components except for the reaction wheel inertia about their respective spin axes. Given that each wheel is aligned along the spin axis $\hat{\mathbf{g}}_i$, the wheel inertia component $\mathbf{H}_s$ can then be expressed by projecting the vector of individual wheel momenta $\mathbf{h}_s$ into the body frame

$$\mathbf{H}_s = [G]\mathbf{h}_s \tag{3}$$

The $3 \times n$ matrix $[G]$ projects the wheel momentum and torque vectors onto the body momentum space, and it is defined in terms of the wheel spin axes as

$$[G] = [\,\hat{\mathbf{g}}_1 \quad \hat{\mathbf{g}}_2 \quad \cdots \quad \hat{\mathbf{g}}_n\,] \tag{4}$$

The wheel momentum vector $\mathbf{h}_s$ is defined in terms of the wheel inertias J_i and spacecraft angular velocities as

$$\mathbf{h}_s = \begin{pmatrix} J_1(\omega_{s,1} + \Omega_1) \\ J_2(\omega_{s,2} + \Omega_2) \\ \vdots \\ J_n(\omega_{s,n} + \Omega_n) \end{pmatrix} \tag{5}$$

where $\omega_{s,i}$ is the component of the spacecraft angular velocity in the ith wheel spin axis, defined as

$$\omega_{s,i} = \boldsymbol{\omega} \cdot \hat{\mathbf{g}}_i \tag{6}$$

The $[\tilde{\omega}]$ is the matrix equivalent of a vector cross product and is defined as

$$[\tilde{\omega}] = \begin{bmatrix} 0 & -\omega_3 & \omega_2 \\ \omega_3 & 0 & -\omega_1 \\ -\omega_2 & \omega_1 & 0 \end{bmatrix} \tag{7}$$

This notation is used to clarify the resulting mathematics, but it can be trivially shown that $[\tilde{\omega}]\mathbf{a} = \boldsymbol{\omega} \times \mathbf{a}$. The n-dimensional wheel torque vector $\mathbf{u}$ is defined as

$$\mathbf{u} = \begin{pmatrix} u_1 \\ u_2 \\ \vdots \\ u_n \end{pmatrix} \tag{8}$$

where u_i is the torque produced by the ith wheel motor. Using these definitions (and neglecting external torques), differentiating Eq. (1) yields the following equation of motion, a reaction-wheel-specific form of Euler's equation [12]

$$[I]\dot{\boldsymbol{\omega}} = -[\tilde{\omega}][I]\boldsymbol{\omega} - [\tilde{\omega}][G]\mathbf{h}_s - [G]\mathbf{u} \tag{9}$$

Control laws derived from this equation specify the control torque term $[G]\mathbf{u}$. The calculation of the wheel torques $\mathbf{u}$ that produce this torque is generally a distinct procedure and is dealt with in detail next.

B. Control Torque Solution

Given the instantaneous spacecraft state, the selected control law specifies the control torque $\mathbf{L}_r$, defined as

$$\mathbf{L}_r = [G]\mathbf{u} \tag{10}$$

at all times. After the desired control torque $\mathbf{L}_r$ is known, it is then necessary to find the combination of wheel torques u_i, which generates this result. One possible solution to Eq. (10) is the L_2 minimum-norm torque $\mathbf{u}^*$ [17]:

$$\mathbf{u}^* = [G]^T([G][G]^T)^{-1}\mathbf{L}_r \tag{11}$$

This solution is not only useful mathematically but also popular for practical application, since wheel motor torques are often a limiting factor, particularly for larger spacecraft.

Since the $\mathbf{L}_r$ torque product is determined by the control law, alternate behaviors can be achieved by altering the solution for the wheel torque vector $\mathbf{u}$. As described above, $\mathbf{u}^*$ is only one possible solution. All other solutions to Eq. (10) are expressed as

$$\mathbf{u} = \mathbf{u}^* + \mathbf{u}_s \tag{12}$$

Since $\mathbf{u}$ must result in the same attitude closed-loop response, the supplementary torque vector $\mathbf{u}_s$ must be in the null space of $[G]$. The null space dimension is $m = n - 3$. Given that the null space of $[G]$ is defined by the m basis vectors $\hat{\mathbf{n}}_i$, the null space matrix $[N]$ is defined as

$$[N] = [\,\hat{\mathbf{n}}_1 \quad \hat{\mathbf{n}}_2 \quad \cdots \quad \hat{\mathbf{n}}_m\,] \tag{13}$$

Using the m-dimensional null space scaling vector $\boldsymbol{\tau}$, the supplementary torque vector can be expressed compactly as

$$\mathbf{u}_s = [N]\boldsymbol{\tau} \tag{14}$$

Any value of $\boldsymbol{\tau}$ results in the same net control torque $[G]\mathbf{u}$. This null space scaling vector is used as the free parameter when developing the power-optimal control below. By this method, the attitude control and supplementary torques are effectively decoupled, allowing for considerable freedom to achieve the desired power-optimal behavior.

This mathematical groundwork can be applied to obtain desirable optimal wheel torque solutions for any given general control law. An instantaneous L_2 power-optimal control, which is the basis for the original work below, was derived by Schaub and Lappas [7], and it is described briefly here for comparison.

To determine the power used by the wheel motors at any instant, the total system kinetic energy K is first expressed as

$$K = \frac{1}{2}\boldsymbol{\omega}^T[I]\boldsymbol{\omega} + \frac{1}{2}\sum_{i=1}^{n} J_i(\Omega_i + \omega_{s,i})^2 \tag{15}$$

Taking the derivative, or applying the work-energy theorem [12], yields the following general expression for total wheel power in the absence of an external torque:

$$P = \sum_{i=1}^{n} \Omega_i u_i \tag{16}$$

However, in a traditional system, power is required to accelerate or decelerate the wheels. The power for such a system is then the product of the wheel speed and torque magnitudes only, regardless of direction, such that

$$P = \sum_{i=1}^{n} |\Omega_i u_i| \tag{17}$$

To minimize this quantity, the control derived in [7] minimizes the L_2 norm of the wheel powers. In this scenario, it takes power to accelerate and decelerate the reaction wheels, and now energy retrieval through wheel speed braking is considered. The following briefly summarizes this approach for easy reference, as the new control performance is later compared with this earlier approach. By defining the vector $\mathbf{P}$ of all of the individual powers $\Omega_i u_i$, a scalar power-squared cost function is defined as

$$J = \tfrac{1}{2}\mathbf{P}^T\mathbf{P} \tag{18}$$

Substituting Eq. (16) and defining $[\Omega] = \mathrm{diag}(\Omega_i)$ gives

$$J = \tfrac{1}{2}([\Omega]\mathbf{u})^T([\Omega]\mathbf{u}) \tag{19}$$

Substituting Eqs. (12) and (14) into the cost function in Eq. (19) results in the following expression to be minimized:

$$J = \tfrac{1}{2}([\Omega](\mathbf{u}^* + [N]\boldsymbol{\tau}))^T([\Omega](\mathbf{u}^* + [N]\boldsymbol{\tau})) \tag{20}$$

For the purposes of instantaneous power-optimal control, $\boldsymbol{\tau}$ is the only free parameter in the cost function, since $[N]$ is a constant, $\mathbf{u}^*$ is governed directly by the desired control torque, and $\boldsymbol{\Omega}$ is a function of the (arbitrary) instantaneous wheel state. Therefore, it is necessary that $\frac{\partial J}{\partial \boldsymbol{\tau}} = \mathbf{0}$ and that $\frac{\partial^2 J}{\partial \boldsymbol{\tau}^2}$ is positive definite to minimize the cost function. Taking the derivative of Eq. (20) and setting it to zero yields

$$[N]^T[\Omega]^2[N]\boldsymbol{\tau} = -[N]^T[\Omega]^2\mathbf{u}^* \tag{21}$$

Assuming that $[N]^T[\Omega]^2[N]$ is invertible, this expression can be solved for $\boldsymbol{\tau}$. There is the potential for a degenerate case in which $\boldsymbol{\Omega} = \mathbf{0}$, causing $[N]^T[\Omega]^2[N]$ to be rank-deficient (in fact, only m wheels must have nonzero spin rates to guarantee full rank). This case may be handled via an alternate formulation, which is omitted here. Finally, the resulting supplementary torque vector $\mathbf{u}_s$ is

$$\mathbf{u}_s = -[N]([N]^T[\Omega]^2[N])^{-1}[N]^T[\Omega]^2\mathbf{u}^* \tag{22}$$

This expression is substituted into Eq. (12) to give the total wheel torque vector.

III. Regenerative Power-Optimal Control

A. Control Derivation

This mathematical approach (based upon the L_2-optimal control above) is applied here to develop a regenerative power-optimal control, so called because power can be regenerated from the wheels. Assuming perfect power return efficiency, the power required to generate this wheel torque at any given set of wheel speeds is simply the summation of the individual wheel powers. In a real system, some power would be lost when decelerating the wheels, but this assumption is made to avoid the discontinuities introduced by the incorporation of a power return efficiency factor. The ideal power function is expressed vectorially as

$$P = \boldsymbol{\Omega}^T\mathbf{u} \tag{23}$$

Substituting Eqs. (12) and (14) into the power equation gives the following regenerative power cost function:

$$P = \boldsymbol{\Omega}^T(\mathbf{u}^* + [N]\boldsymbol{\tau}) \tag{24}$$

At any arbitrary point in time, $\boldsymbol{\Omega}$ is a function of the instantaneous state and cannot be altered. Similarly, $\mathbf{u}^*$ is a function only of the instantaneous state, and $[N]$ is a constant. The power is then only a function of an arbitrary null space vector $\boldsymbol{\tau}$. Since $\boldsymbol{\tau}$ is the only free parameter, Eq. (24) is a linear function representing an m-dimensional hyperplane, the slope of which is a function only of the wheel geometry and wheel speeds.

The function is linear, so the direction of the power extrema at any point can be found by calculating the gradient of this plane, keeping in mind that all parameters except $\boldsymbol{\tau}$ are fixed:

$$\nabla P = \frac{\partial P}{\partial \boldsymbol{\tau}} = \boldsymbol{\Omega}^T[N] \tag{25}$$

The extrema of the power plane lie along the gradient direction, so $\boldsymbol{\tau}_s$ (the extremizing value of $\boldsymbol{\tau}$) can be expressed in terms of the gradient (and m-dimensional vector in the null space) and an unknown scalar multiplier α

$$\boldsymbol{\tau}_s = \alpha \nabla P^T = \alpha[N]^T\boldsymbol{\Omega} \tag{26}$$

where $\boldsymbol{\tau}_s$ is a column vector, so ∇P is transposed since the result of Eq. (25) is a $1 \times m$ matrix containing the gradient vector elements. This geometry is shown in the null space (for an $m = 2$ case) in Fig. 2.

With the extremizing null space vector $\boldsymbol{\tau}_s$ defined in Eq. (26), the corresponding extremizing supplementary wheel torque vector $\mathbf{u}_s$ can be found from Eq. (14). Substituting the definition of $\boldsymbol{\tau}_s$ in Eq. (26) gives the following expression for $\mathbf{u}_s$ in terms of the unknown scalar α:

$$\mathbf{u}_s = \alpha[N][N]^T\boldsymbol{\Omega} \tag{27}$$

It can be seen in Eq. (27) that $\mathbf{u}_s$ is an n-dimensional line in the power function gradient direction. The scalar multiplier α must then be chosen to maximize the magnitude of $\mathbf{u}_s$, thereby maximizing the change in power use. However, based on this information alone, the power extrema appear to lie at $\alpha = \pm\infty$. This is neither physically possible nor desirable, so the magnitude of $\mathbf{u}_s$ must be maximized subject to a set of constraints: the physical limits on the wheel motor torques. Given that the ith motor can exert a maximum torque of $B_{h,i}$ and a minimum (negative direction) torque of $B_{l,i}$, each wheel torque u_i must satisfy

$$B_{l,i} \le u_i \le B_{h,i} \tag{28}$$

Each torque bound creates two bounding hyperplanes at $u_i = B_{l,i}$ and $u_i = B_{h,i}$. It can be assumed for most motors that $B_{h,i} = B_{l,i}$, but the separate values are preserved here for generality.

The $2n$ values of α corresponding to each set of torque-bound planes are calculated by finding the intersections of the gradient line with the bounding hyperplanes. For each pair of bounding planes, the points of intersection are found at

$$u_i^* + u_{s,i} = B_{h,i} \qquad u_i^* + u_{s,i} = B_{l,i} \tag{29}$$

By defining T_i as the ith element of the $[N]\boldsymbol{\tau}$ torque space gradient vector and substituting Eq. (27), Eq. (29) becomes

$$u_i^* + \alpha T_i = B_{h,i} \qquad u_i^* + \alpha T_i = B_{l,i} \tag{30}$$

Rearranging gives the two α values for the ith motor bounding hyperplane intersection with the low- and high- torque bounds, denoted $\alpha_{l,i}$ and $\alpha_{h,i}$, respectively:

$$\alpha_{l,i} = \frac{B_{l,i} - u_i^*}{T_i} \qquad \alpha_{h,i} = \frac{B_{h,i} - u_i^*}{T_i} \tag{31}$$

It is also apparent that at least one of the motor torques will always be saturated, since the torque vector is now defined such that it intersects one of the maximum torque bounding planes z. The wheel torque bounding planes and the corresponding gradient direction intersections are shown in Fig. 3, given a four wheel case ($m = 1$) with arbitrary wheel rates and arbitrary $\mathbf{L}_r$, showing the intersection with the plane corresponding to each potential α value. The four-dimensional wheel torque space is projected onto two separate two-dimensional planes for easy visualization.

The surface that satisfies all of these constraints then forms an n-dimensional hypercube, and the extrema of the cost function (the maximum supplementary torque vector magnitudes) are found at the intersection of $\mathbf{u}_s$ with this hypercube. If the minimum-norm torque $\mathbf{u}^*$ satisfies the torque constraint, there are only two possible intersections of $\mathbf{u}_s$ with the bounding hypercube (a convex polyhedron). This is a safe assumption, since a $\mathbf{u}^*$ that violated the torque constraints would no longer guarantee stability, and it would indicate a fundamental problem with the control gain selection. In practice, these two intersections are found by testing every possible $\alpha_{l,i}$ and $\alpha_{h,i}$ solution against every constraint. Figure 4 shows the two possible supplementary torque vectors that satisfy all of the constraints. In this example, it is apparent that the limiting torque hyperplanes (the sides of the hypercube with which $\mathbf{u}_s$ intersects) are $u_2 = B_{l,2}$ and $u_4 = B_{h,4}$. When numerically implemented, it can be safely assumed that only two α values will be found, since more than two values can only occur if $\mathbf{u}_s$ passes through an edge or corner of the hypercube (this is a result of testing the bounding planes individually), and a solution falling precisely on an edge or corner is unlikely. Even in the event that this did occur, resulting in more than two possible α values, only two of the values would be distinct, and one of the repeated values could be selected arbitrarily. Only the distinct values $\alpha_{1,2}$ are dealt with next.

The resulting two α values now generate the maximum and minimum possible instantaneous power use. Additionally, it is apparent from the geometry in Fig. 4 that $\alpha_1 \le 0$ and $\alpha_2 \ge 0$, assuming that $\mathbf{u}^*$ satisfies the torque constraints. Since α_1 moves in the negative gradient direction and α_2 moves in the positive gradient direction, α_1 and α_2 correspond to the minimum and maximum power, respectively. This may be easily verified by substitution into the original power equation. From Eqs. (27) and (12), the wheel torque vector is

$$\mathbf{u}_{1,2} = \mathbf{u}^* + \alpha_{1,2}[N][N]^T\boldsymbol{\Omega} \tag{32}$$

Substituting Eq. (32) into Eq. (24) gives

$$P_{1,2} = \boldsymbol{\Omega}^T(\mathbf{u}^* + \alpha_{1,2}[N][N]^T\boldsymbol{\Omega}) \tag{33}$$

The product $\boldsymbol{\Omega}^T[N][N]^T\boldsymbol{\Omega}$ is nonnegative scalar, confirming by inspection that $\max(\alpha_{1,2})$ corresponds to $P_{\max}$, and $\min(\alpha_{1,2})$ corresponds to $P_{\min}$. Selecting α_1 gives the final minimum power wheel torque as

$$\mathbf{u} = \mathbf{u}^* + \alpha_1[N][N]^T\boldsymbol{\Omega} \tag{34}$$

Like the other instantaneous power-optimal control above, this can be applied to any control law generating an instantaneous desired $\mathbf{L}_r$ control torque.

Since α_1 and α_2 generate the minimum and maximum possible power solutions, any α satisfying

$$\alpha_1 \le \alpha \le \alpha_2 \tag{35}$$

is also admissible. According to Eq. (33), power varies linearly with α, so a range of wheel motor total powers between P_1 and P_2 is available at any instant, as shown in Fig. 5. This property is useful to modify the control's power behavior, and the potential application for power tracking and IPACS is discussed briefly below.

B. Numerical Implementation

While the control formulation presented above is free of mathematical singularities, there are numerical issues that must be dealt with. As the excess system energy approaches zero, the power hyperplane in Eq. (24) flattens and the gradient approaches $\mathbf{0}$. As the norm of the gradient becomes critically small, machine roundoff error begins to dominate the gradient vector, causing rapid changes in ∇P and corresponding sign changes in the two α solutions. The resulting chatter behavior, shown in Fig. 6a, is undesirable for any practical application, even though the resulting control torque is unaffected. Not only would this create unnecessary mechanical stresses, but such oscillations would be more likely to excite undesirable elastic modes in the spacecraft [4]. Note that the wheels oscillate between the saturated torques at ± 1 Nm. Since the regenerative control is always saturated, it is a type of bang–bang control law. As such, this behavior can easily be alleviated by adding a deadband under which α_1 is set to zero. This is easily implemented

Table 1 Numerical simulation parameters

Initial state	Values
A	$\boldsymbol{\sigma}_0 = \mathbf{0}$, $\boldsymbol{\omega}_0 = [0 \quad 1 \quad 2]^T$ rpm, $\boldsymbol{\Omega}_0 = [500 \quad 500 \quad 500 \quad 200]^T$ rpm
B	$\boldsymbol{\sigma}_0 = [0 \quad 0.5 \quad 0.2]^T$, $\boldsymbol{\omega}_0 = \mathbf{0}$ rpm, $\boldsymbol{\Omega}_0 = [500 \quad 500 \quad 500 \quad 500]^T$ rpm

by using the magnitude of ∇P as the relevant scalar measure to which the deadband can be applied. Using the deadband value ϵ, this is expressed as

$$|\nabla P| < \epsilon \Rightarrow \alpha_1 = 0 \tag{36}$$

The effect of implementing the deadband is shown in Fig. 6b. The resulting motor torques are much better behaved, with the rapid oscillations between saturated states completely removed. The selection of ϵ is somewhat arbitrary but may be set to a relatively large value ($\epsilon = 0.3$ is used above) since it has little impact on power performance and total energy return. For example, in the configuration used above, increasing the deadband by an order of magnitude from $\epsilon = 0.3$ to $\epsilon = 3$ engages the deadband 0.2 s earlier, and it only reduces the total energy returned by 0.3 J.

IV. Numerical Simulations

A. System Definition

The simulations below are performed with a four-wheeled craft with an inertia of

$$\text{diag}\,(5, 5, 8)\ \text{kg} \cdot \text{m}^2$$

The reaction wheels all have a spin axis inertia of $J_i = 0.1\ \text{kg} \cdot \text{m}^2$. The torque boundary for all wheel motors is $B_{h,i} = -B_{l,i} = 1$ Nm. Two different sets of spacecraft initial angular velocities and wheel speeds are used: each chosen to accentuate different behavior characteristics. Initial state A has perturbed angular velocity (for the velocity regulation simulations), and initial state B has a perturbed initial attitude and angular velocity (for the tracking control simulations). The elements of the $\boldsymbol{\sigma}$ vector are the modified Rodrigues parameters (MRPs) [18–20] giving the attitude of the $\mathcal{B}$ frame with respect to the $\mathcal{N}$ frame (see Table 1).

The four wheels are arranged in a tripod configuration, shown in Fig. 1. This is a popular redundant wheel configuration, since the fourth wheel can be used to generate an arbitrary three-axis control torque in the event that any of the first three orthogonal wheels fails. The corresponding $[G]$ for this geometry is

$$[G] = \begin{bmatrix} 1 & 0 & 0 & -1/\sqrt{3} \\ 0 & 1 & 0 & -1/\sqrt{3} \\ 0 & 0 & 1 & -1/\sqrt{3} \end{bmatrix} \tag{37}$$

Since this configuration has four wheels ($n = 4$), there is a one-dimensional null space ($m = 1$) with the basis vector

$$\hat{\mathbf{n}}_1 = \begin{bmatrix} 1/\sqrt{3} \\ 1/\sqrt{3} \\ 1/\sqrt{3} \\ 1 \end{bmatrix} \tag{38}$$

Integration of the equations of motion given in Eq. (9) is performed using a fourth-order Runge–Kutta integration scheme.

B. At-Rest Power Minimization

In this simulation, the spacecraft is initially at rest, and the velocity regulator control law below is implemented:

$$[G]\mathbf{u} = P\boldsymbol{\omega} - [\tilde{\omega}]([I]\boldsymbol{\omega} + [G]\mathbf{h}_s) \tag{39}$$

The scalar gain P is set to 1.2, although the control law is unimportant for this simulation, since the initial angular velocity is zero, resulting in a control torque $\mathbf{L}_r$ that is always zero. Thus, only null motion torques are applied to the wheels in order to return energy from them. The standard minimum-norm regulator control $\mathbf{u} = \mathbf{u}^*$, which does not use any null motion and remains inactive, is included for a point of reference. The simulated control performance is illustrated in Fig. 7, beginning at initial state B.

Figure 8 shows the wheel rates over the duration of the simulations, which reach their steady-state values as the return power goes to zero. Both controls keep the spacecraft at rest, generating zero net control torque. While the standard regulator applies no wheel torque, the regenerative regulator returns energy from the wheels. Since the goal of the wheel null motion is to extract the maximum amount of power from the wheels at all times, it follows that the wheels ought to reach their minimum energy state as $t \to \infty$. The minimum wheel speed can be calculated analytically by determining the minimum energy solution that satisfies conservation of momentum in the inertial frame.

Assuming that all of the wheels have the same inertia J, application of Eq. (15) gives the following expression for the total kinetic energy K:

$$K = \frac{1}{2}\boldsymbol{\omega}^T[I]\boldsymbol{\omega} + \frac{1}{2}J\sum_{i=1}^{4}(\Omega_i + \omega_{s,i})^2 \tag{40}$$

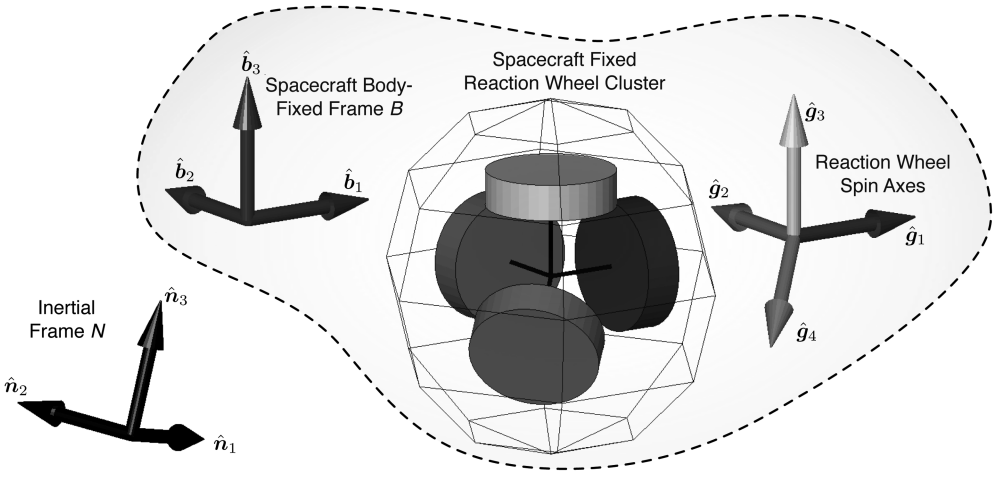

Fig. 1 Tripod configuration of four reaction wheels.

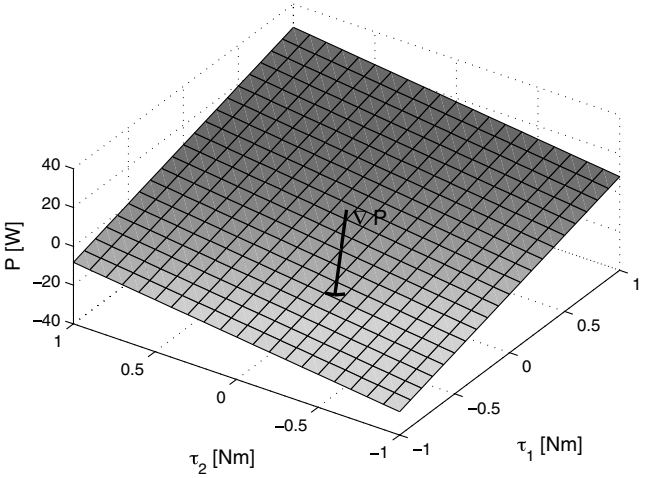

Fig. 2 Power hyperplane and gradient in a two-dimensional sample null space of [G].

Using these terms, the spacecraft angular momentum is expressed as

$$\mathbf{H} = [I]\boldsymbol{\omega} + [G]\mathbf{h} \tag{41}$$

Given that the spacecraft is initially at rest with angular momentum $\mathbf{H_0} = [\,h_1 \quad h_2 \quad h_3\,]^T$, and using Eq. (41) with the wheel configuration in Eq. (37), the wheel speeds are related to the initial angular momentum by

$$\begin{pmatrix} h_1 \\ h_2 \\ h_3 \end{pmatrix} = J \begin{pmatrix} \Omega_1 - 1/\sqrt{3}\Omega_4 \\ \Omega_2 - 1/\sqrt{3}\Omega_4 \\ \Omega_3 - 1/\sqrt{3}\Omega_4 \end{pmatrix} \tag{42}$$

Substituting this result into Eq. (40) gives the following expression for total kinetic energy:

$$K = J\frac{1}{2}\left(\left(\frac{h_1}{J} + \frac{\Omega_4}{\sqrt{3}}\right)^2 + \left(\frac{h_2}{J} + \frac{\Omega_4}{\sqrt{3}}\right)^2 + \left(\frac{h_3}{J} + \frac{\Omega_4}{\sqrt{3}}\right)^2 + \Omega_4^2\right) \tag{43}$$

Because $\mathbf{H}_0$ remains constant in the absence of external torque, setting the derivative of Eq. (43) to zero and solving for Ω_4 yields the following minimum energy wheel speeds:

$$\begin{pmatrix} \Omega_1 \\ \Omega_2 \\ \Omega_3 \\ \Omega_4 \end{pmatrix} = -\frac{1}{J} \begin{pmatrix} \frac{h_2+h_3-5h_1}{6} \\ \frac{h_1+h_3-5h_2}{6} \\ \frac{h_1+h_2-5h_3}{6} \\ \frac{h_1+h_2+h_3}{\sqrt{12}} \end{pmatrix} \tag{44}$$

These results are somewhat more complex for the more general case of varying wheel inertias and nonzero spacecraft initial velocity, but the same analysis applies. Evaluating Eq. (44) with the initial

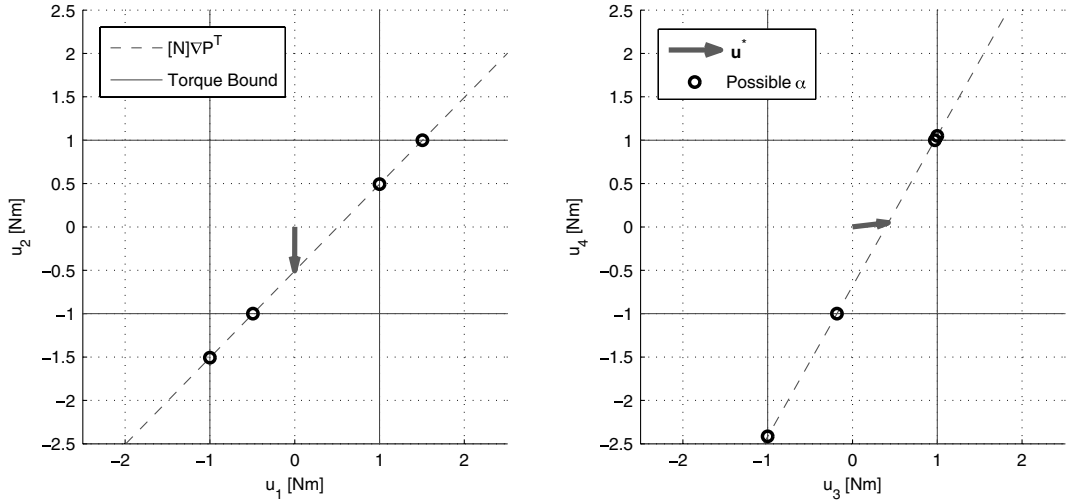

Fig. 3 Gradient line-bounding plane intersection.

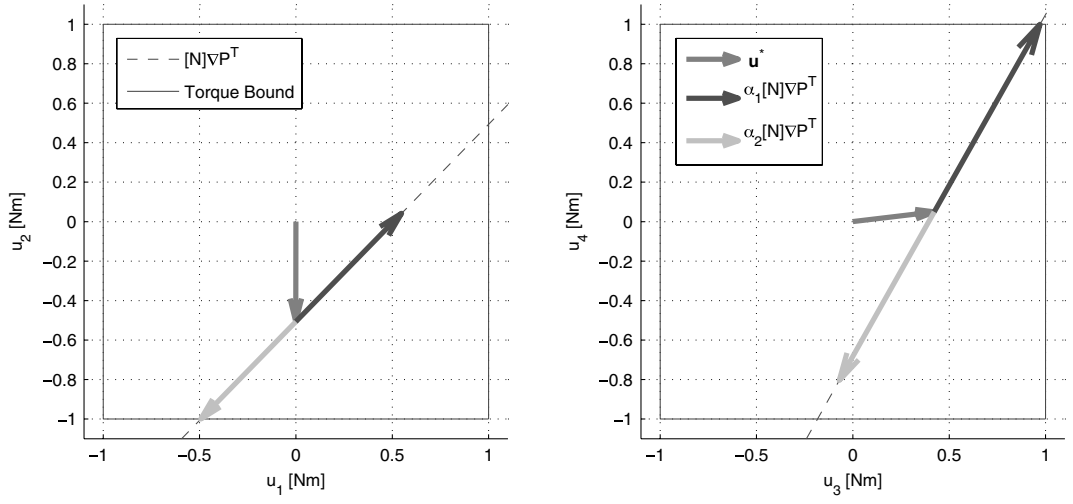

Fig. 4 Supplementary torque vector–hypercube intersection.

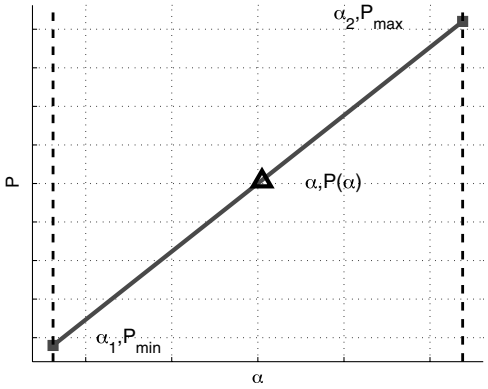

Fig. 5 Instantaneous power range.

conditions given above gives the theoretical minimum wheel spin rates for this configuration:

$$\left.\begin{pmatrix}\Omega_1\\ \Omega_2\\ \Omega_3\\ \Omega_4\end{pmatrix}\right|_{\min(K)} = \begin{pmatrix}11.06\\ 11.06\\ 11.06\\ -19.17\end{pmatrix} \text{ rad/s} \tag{45}$$

As expected, all of the wheel rates in Fig. 8 approach the values predicted in Eq. (45). At this point, the minimum energy state has been reached, and no power can be returned from the wheels. This minimum-energy-state-seeking behavior is desirable from a wheel-speed-management standpoint. However, due to potential wheel stickage issues, the zero wheel speed crossing may be undesirable for some systems.

C. Regulation Power Minimization

In this simulation, the spacecraft is given a substantial initial angular velocity, starting at initial state A. The same regulator control in Eq. (39) is implemented, and the performance is illustrated in Fig. 9. Two other controls are shown for comparison: minimum-norm control equation (11), and L_2 power-optimal control equation (22). Both of the power-optimal controls consume less power than the minimum-norm control. While the regenerative regulator control returns considerably more power initially, it is eventually surpassed by the L_2-optimal control. This is a result of the fact that both controls only guarantee instantaneous power-optimal behavior. As shown in Fig. 10, the two power-optimal controls result in very different wheel rate time histories. This illustrates that, while the regenerative control guarantees optimal power return for any instantaneous set of wheel rates, it is not necessarily superior to the L_2-optimal control at all points during the maneuver. However, the regenerative control can still be expected to extract more energy from the wheels for any arbitrary maneuver, since it has been defined to produce the maximum power return from the wheels given any instantaneous state. This is confirmed by integration of the power histories show in Fig. 9; the L_2-optimal control returns 95.3 J, while the regenerative control returns 163.7 J.

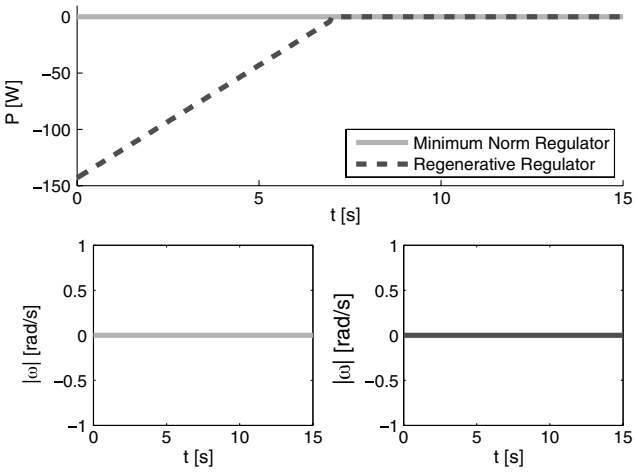

Fig. 7 Regulator control power comparison, $\omega_0 = 0$.

The same minimum-energy-state-seeking behavior seen in Fig. 7 is also seen for the nonzero initial spacecraft angular velocity. Figure 11 shows the total system kinetic energy, as calculated from Eq. (15). Also, since the regenerative control is always saturated, higher wheel torques are expected at all times. By definition, both of the power-optimal controls will produce larger wheel torques than the minimum-norm control (Fig. 12).

D. Tracking Power Minimization

While all of the controls above have been velocity regulators, the control law implemented below tracks a specific attitude and angular velocity profile, starting at initial state B. In this simulation, the MRP attitude $\boldsymbol{\sigma}_r$ and angular velocity $\boldsymbol{\omega}_r$ of frame $\mathcal{R}$ are tracked by the control

$$[G]\mathbf{u} = K\boldsymbol{\sigma}_\delta + P\delta\boldsymbol{\omega} - [\tilde{\omega}]([I]\boldsymbol{\omega} + [G]\mathbf{h}_s - \boldsymbol{\omega}_r) - [I](\dot{\boldsymbol{\omega}}_r - [\tilde{\omega}]\boldsymbol{\omega}_r) \tag{46}$$

where $\boldsymbol{\sigma}\delta$ and $\delta\boldsymbol{\omega}$ are the errors between the $\mathcal{B}$ and $\mathcal{R}$ frame attitudes and angular velocities, respectively. The selected angular velocity error and attitude error gains are, respectively, $P = 1.2$ and $K = 0.3$. These frames are shown in Fig. 13.

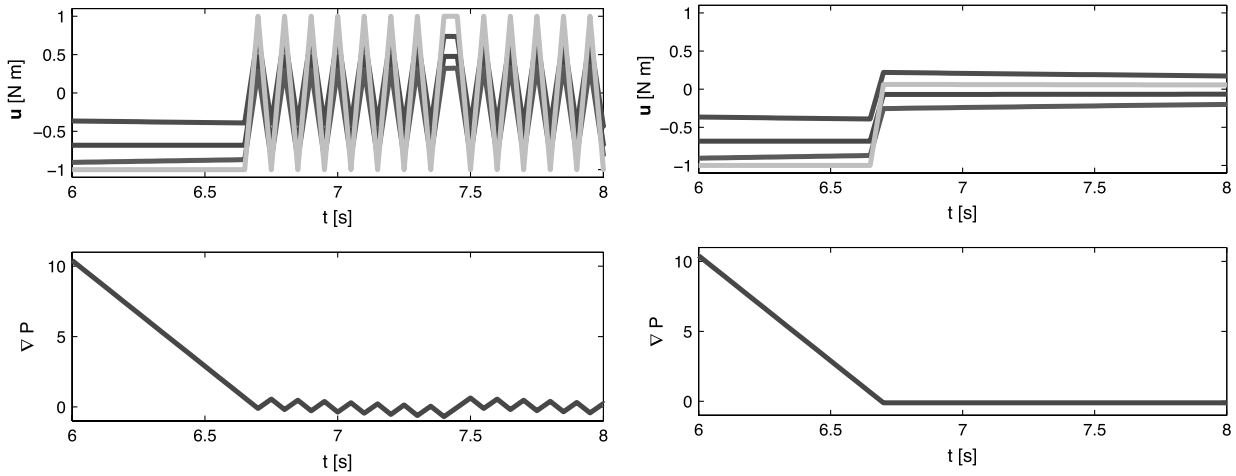

a) Wheel Torque Chatter **b) Chatter Removal Using $\epsilon = 0.3$ Deadband**

Fig. 6 Deadband application to alleviate chatter.

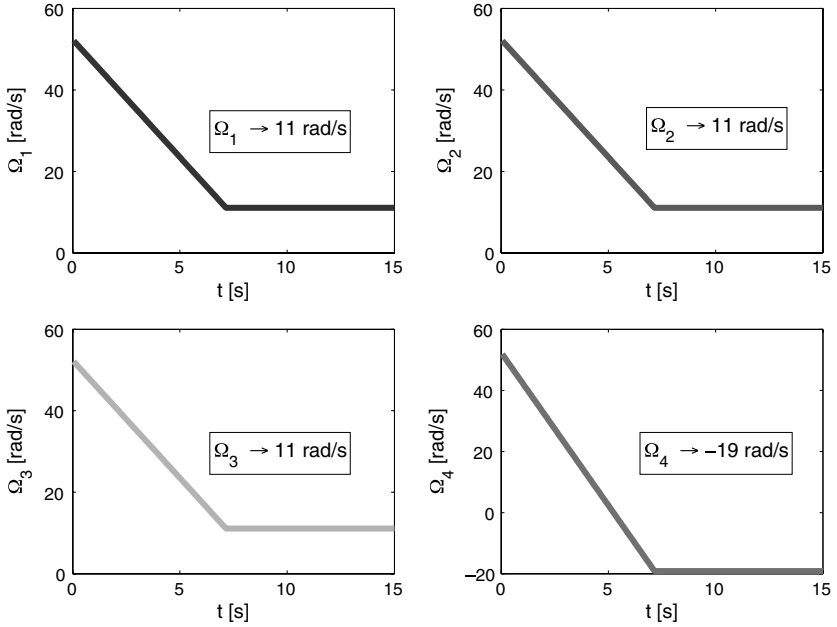

Fig. 8 Regulator control wheel speed comparison, $\omega_0 = 0$.

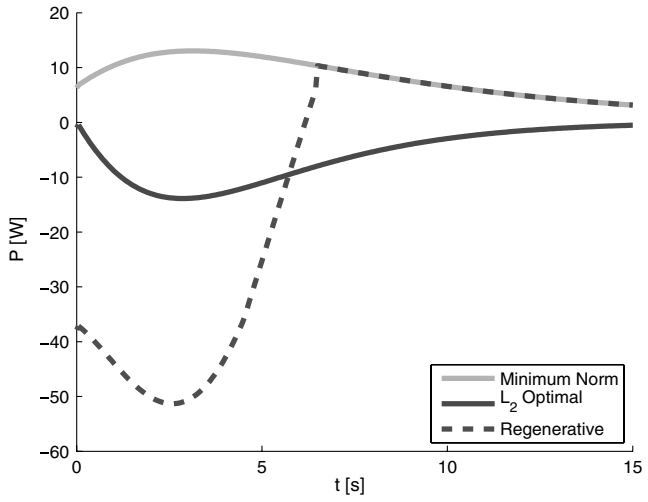

Fig. 9 Regulator control power comparison, perturbed ω_0.

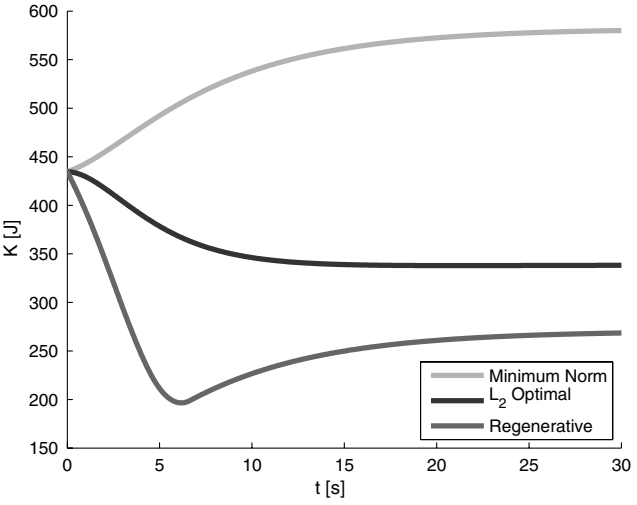

Fig. 11 Total kinetic energy comparison.

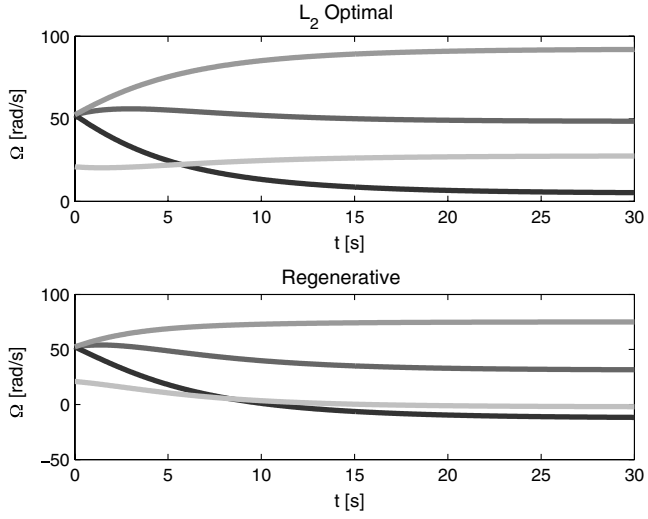

Fig. 10 Power-optimal control Ω comparison.

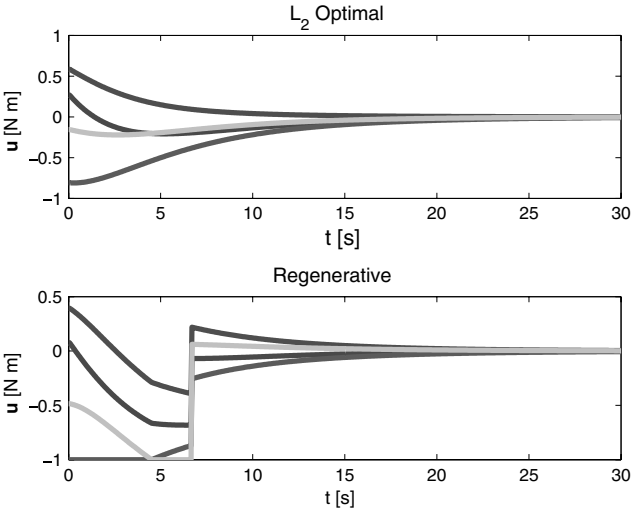

Fig. 12 Power-optimal control u comparison.

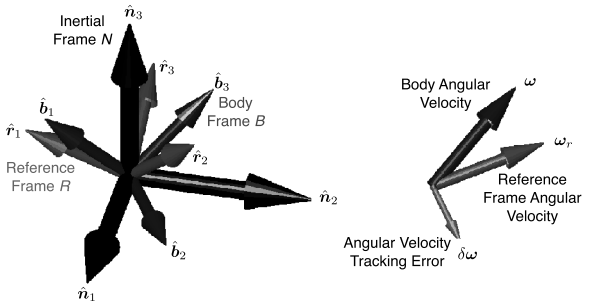

Fig. 13 Tracking control reference frames.

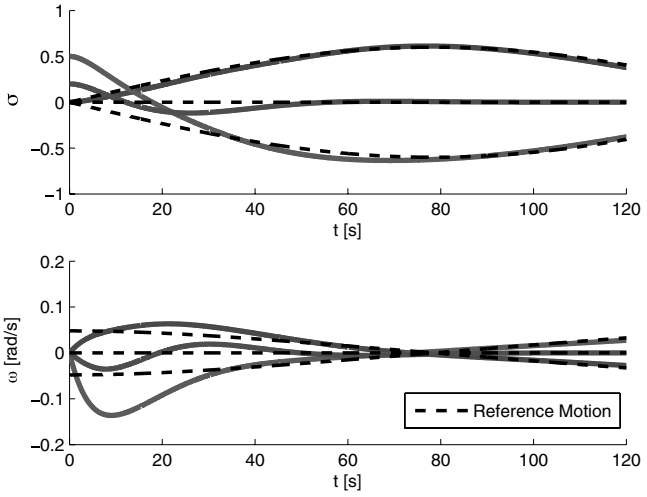

Fig. 14 Minimum-norm tracking control.

In Fig. 14, the minimum-norm wheel torque solution is implemented, tracking the attitude history

$$\boldsymbol{\sigma}_r = [\,0.3\sin(0.02t) \quad -0.3\sin(0.02t) \quad 0\,]^T$$

The corresponding reference angular velocity is calculated by applying MRP kinematic relations to the easily differentiable attitude history, giving [12]

$$\boldsymbol{\omega}_r = \tfrac{1}{4}[(1-\boldsymbol{\sigma}_r^T\boldsymbol{\sigma}_r)[I_{3\times3}] + 2[\tilde{\sigma}_r] + 2\boldsymbol{\sigma}_r\boldsymbol{\sigma}_r^T]^{-1}\dot{\boldsymbol{\sigma}}_r \qquad (47)$$

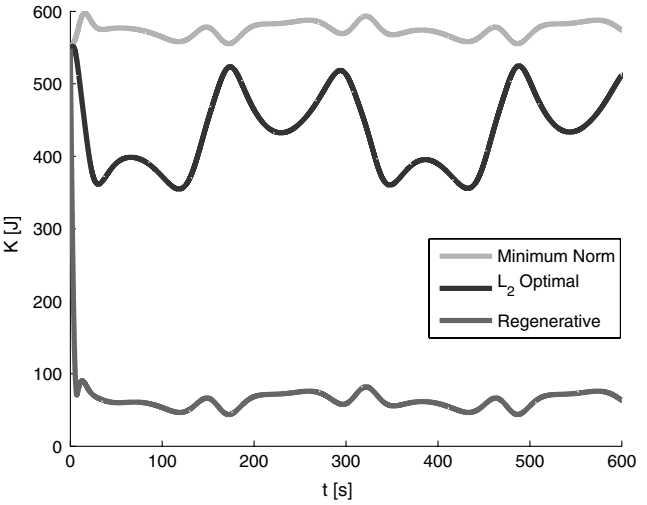

Fig. 16 Total kinetic energy comparison.

As mentioned above, the selection of the wheel torque solutions does not affect the performance characteristics of the control, so the power-optimal controls exhibit exactly the same behavior. The power behavior is much the same as seen in the regulator control above. Here, the same control law is applied using the minimum-norm, L_2-optimal, and regenerative wheel torque solutions. Figure 15a shows the first 30 s of the simulation. Exactly as seen in the velocity regulator control, the regenerative control initially returns a large amount of power as excess energy is removed from the system. Again, since both controls guarantee only instantaneous power-optimality, neither can be said to always perform better than the other. Figure 15b shows the remainder of the simulation, in which initial condition effects have largely vanished. Two behaviors are apparent here. First, the L_2-optimal control is no longer power-optimal because of the altered power calculation; this was also the case in the regulator control above, but it could not be illustrated since the control torque approached zero. Second, once it falls within the power plane gradient deadband, the regenerative power-optimal control behaves identically to the minimum-norm control.

To further understand the behavior of the three controls, it is useful to compare the evolution of the total system energy as given in Eq. (15). This is shown in Fig. 16. Since torque is applied to the system, energy is no longer conserved, but the regenerative control still exhibits the minimum-energy-state-seeking behavior explored above. This also explains the lack of power-optimal performance

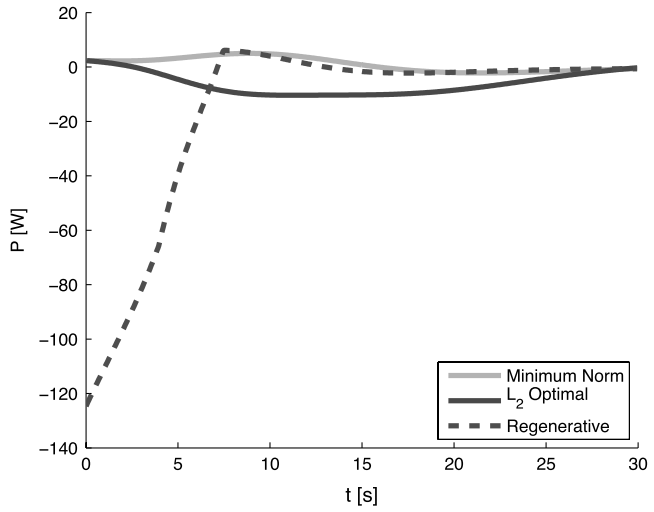

a) 0 to 30 seconds

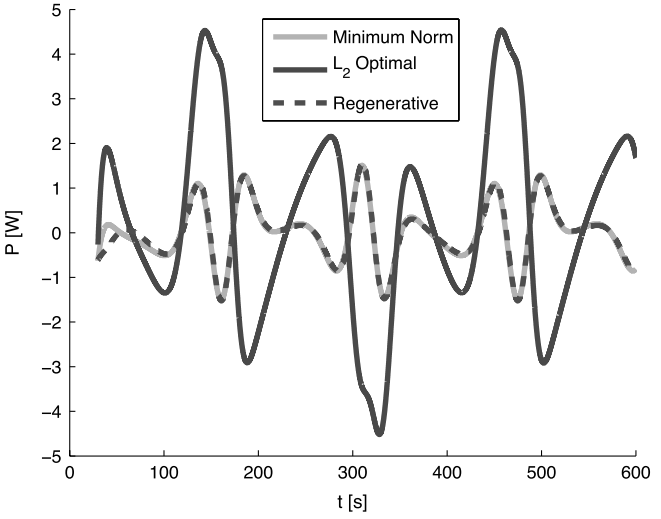

b) 30 to 600 seconds

Fig. 15 Tracking power comparison.

from the L_2-optimal control seen in Fig. 15b, since its wheel state behavior left the system at a much higher total energy.

V. Conclusions

The new control law provides a method to minimize instantaneous power usage for a redundant reaction wheel attitude control system using flywheels for energy return. By expressing the total power as a linear function of the reaction wheel torque null space, the power-optimal wheel torque is determined analytically while considering reaction wheel torque saturation constraints. The formulation is applicable to any number of redundant wheels in any arbitrary geometry (which spans three-dimensional space). A potential numerical issue, which results in undesirable motor chatter behavior often seen in similar saturated bang–bang control laws, is eliminated by application of a simple deadband strategy.

Numerical simulations illustrate that the control has the expected identical attitude control performance to other attitude control solutions while demonstrating favorable power-optimal characteristics. An important behavior apparent throughout the simulations was the minimum energy state seeking, by which all excess energy is returned from the wheels, providing desirable power return and wheel speed management. By this mechanism. the control not only results in instantaneous power-optimal behavior, but this wheel speed steering law also incorporates the previously used practice of keeping the overall wheel speeds low to reduce the power requirements.

References

[1] Larson, W. H., and Wertz, J. L. (eds.), *Space Mission Analysis and Design*, 3rd ed., Microcosm Press, Portland, OR, 1999, p. 369.

[2] Sarsfield, L., *The Cosmos on a Shoestring: Small Spacecraft for Earth and Space Science*, RAND, Santa Monica, CA, 1998, pp. 7–21.

[3] Tsiotras, P., Shen, H., and Hall, C., "Satellite Attitude Control and Power Tracking with Energy/Momentum Wheels," *Journal of Guidance, Control, and Dynamics*, Vol. 24, No. 1, 2001, pp. 23–24. doi:10.2514/2.4705

[4] Skaar, S., and Kraige, L., "Large-Angle Spacecraft Attitude Maneuvers Using an Optimal Reaction Wheel Power Criterion," *Journal of the Astronautical Sciences*, Vol. 32, No. 1, 1984, pp. 47–61.

[5] Fausz, J. L., and Richie, D. J., "Flywheel Simultaneous Attitude Control and Energy Storage Using a VSCMG Configuration," *Proceedings of the 2000 IEEE International Conference on Control Applications*, IEEE, Piscataway, NJ, Sept. 2000, pp. 991–995.

[6] Grassi, M., and Pastena, M., "Minimum Power Optimal Control of Microsatellite Attitude Dynamics," *Journal of Guidance, Control, and Dynamics*, Vol. 23, No. 5, 2000, pp. 798–804. doi:10.2514/2.4640

[7] Schaub, H., and Lappas, V. J., "Redundant Reaction Wheel Torque Distribution Yielding Instantaneous L_2 Power-Optimal Attitude Control," *Journal of Guidance, Control, and Dynamics*, Vol. 32, No. 4, 2009, pp. 1269–1276. doi:10.2514/1.41070

[8] Hall, C. D., "High Speed Flywheels for Integrated Energy Storage and Attitude Control," *Proceedings of the 1997 American Control Conference*, IEEE, New York, June 1997, pp. 1894–1898.

[9] Pieronek, T. J., Decker, D. K., and Spector, V. A., "Spacecraft Flywheel Systems: Benefits, and Issues," *Proceedings of the IEEE 1997 National Aerospace and Electronics Conference*, IEEE, Piscataway, NJ, July 1997.

[10] Smay, J. W., "Spacecraft Energy Storage, Attitude Steering, and Momentum Management System," U.S. Patent 5,611,505, 18 March 1997.

[11] Eisenhaure, D. B., Downer, J. R., Bliamptis, T. E., Oberbeck, G. A., and Hendrie, S. D., "Energy Storage and Attitude Control Reference System," U.S. Patent 4,723,735, 9 Feb. 1988.

[12] Junkins, J., and Schaub, H., *Analytical Mechanics of Space Systems*, 2nd ed., AIAA, Reston, VA, 2009, pp. 122, 159, 178–187, 419–430.

[13] Choi, Y., Leeghim, H., and Bang, H., "Efficient Control Torque Distribution Approach for Spacecraft Attitude Control," 2008 Guidance, Navigation and Control Conference, AIAA Paper 2008-7234, Aug. 2008.

[14] Richie, D. J., Lappas, V. J., and Palmer, P. L., "Sizing/Optimization of a Small Satellite Energy Storage and Attitude Control System," Univ. of Surrey, TR ADA447543, Guilford, England, U.K., 14 April 2006.

[15] Goodzeit, N. E., and Linder, D. M., "Wheel Speed Management Control System for Spacecraft," U.S. Patent 5,058,835, 22 Oct. 1991.

[16] Ratan, S., and Li, X., "Optimal Speed Management for Reaction Wheel Control System and Method," U.S. Patent 7,198,232, 3 April 2007.

[17] Brogan, W. L., *Modern Control Theory*, 3rd ed., Prentice–Hall, Upper Saddle River, NJ, 1991, p. 220.

[18] Wiener, T. F., *Theoretical Analysis of Gimballess Inertial Reference Equipment Using Delta-Modulated Instruments*, Ph.D. Dissertation, Department of Aeronautics and Astronautics, Massachusetts Inst. of Technology, Cambridge, MA, March 1962.

[19] Marandi, S. R., and Modi, V. J., "A Preferred Coordinate System and the Associated Orientation Representation in Attitude Dynamics," *Acta Astronautica*, Vol. 15, No. 11, 1987, pp. 833–843. doi:10.1016/0094-5765(87)90038-5

[20] Schaub, H., and Junkins, J. L., "Stereographic Orientation Parameters for Attitude Dynamics: A Generalization of the Rodrigues Parameters," *Journal of the Astronautical Sciences*, Vol. 44, No. 1, 1996, pp. 1–19.